

Quantum network sensing with efficient multi-partite entanglement distribution via lossy channels

Yoshihiro Ueda^{1,*}, Makoto Ishihara¹, Wojciech Roga¹, and Masahiro Takeoka^{1,2}

¹*Department of Electronics and Electrical Engineering, Keio University,
3-14-1 Hiyoshi, Kohoku-ku, Yokohama 223-8522, Japan and*

²*Advanced ICT Research Institute, National Institute of Information and
Communications Technology (NICT), Koganei, Tokyo 184-8795, Japan*

(Dated: June 12, 2025)

Quantum network sensing shows potential to enhance the estimation precision for functions of spatially distributed parameters beyond the shot noise limit. The key resource required for this task is possibly multi-partite quantum entanglement. The photonic entanglement is the most natural for this task; however, distributing it over long distances presents significant difficulties, mainly because of unavoidable loss in communication channels. In this research, we analyze a quantum network sensing protocol based on a recently proposed, efficient GHZ state distribution scheme. In comparison to conventional methods based on entanglement distribution, our protocol shows the decreasing loss-induced estimation error of certain functions of distributed parameters including their arbitrary linear combinations.

I. INTRODUCTION

Entanglement based quantum sensing [1–3] is known as a sensing method which can surpass the classical limit in terms of measurement precision. Specifically, measuring a parameter θ repeatedly with M classical probes, such as light pulses, results in the estimation error scaling according to the so-called Standard Quantum Limit (SQL), $1/\sqrt{M}$. In contrast, by using the quantum entangled probe M times, the estimation error scaling becomes $1/M$, referred as the Heisenberg Limit (HL) [4, 5]. This can appear advantageous in various applications ranging from microscopy [6] to gravitational wave detection [7] in which the number of probes is naturally limited. Moreover, quantum-enhanced network sensing aiming at a precise estimation of multiple parameters $\theta_i (i = 1, \dots, M)$ and their linear combinations, $\bar{\theta} = \sum_i^M w_i \theta_i$ can be applicable in quantum network scenarios [8–10] such as precise clock synchronization [11, 12] and the long-baseline quantum telescope [13–15].

Recent results show that both the continuous variable (CV) [16–18] and discrete variable (DV) [19–21] multi-partite entanglement can be useful in enhanced-precision phase estimation with respect to the classical methods. In particular, Greenberger-Horne-Zeilinger (GHZ) states [22] are known to be the optimal probes which can attain the Heisenberg limit [2]. In addition, exceeding the classical limit based on CV [23, 24] and DV [25–28] entanglement was also observed experimentally.

Although several research papers have estimated the performance of quantum network sensing including the effect of noisy environment [29–31], the entanglement distribution process with long-distance lossy communication channels is rarely included in the analysis. The aim of our study is to fill this gap and propose and analyze a

feasible protocol for near-term quantum network sensing which includes the entanglement distribution process.

We assume that the distributed sensing system consists of several sensing stations connected in a network via optical fibers characterized by a given transmittance per km. We assume the star network configuration, as in Fig. 1.

In such a setup, the entangled state could be distributed in several ways. Let us first mention the standard approaches that will become our references. In the first approach, the multi-partite entanglement could be created by sharing photonic bi-partite entanglement between the sensing stations and the central station followed by a multipartite entanglement distillation process. The second approach, which we call direct transmission, would consist of generation of a multi-photon entangled state in the central station followed by its transferring to the sensing stations by the optical fibers, see Fig. 1 *a*). However, if the entanglement is to be distributed to M sensor stations through the optical links, all photons must be successfully transmitted. If the transmission rate is η , the probability of this process scales as $\mathcal{O}(\eta^M)$. It is especially critical for long distance transfers, in which case $\eta \ll 1$, and the robustness of the distribution protocol against loss becomes essential.

In this paper, we propose the distributed sensing protocol with efficient GHZ state distribution [32], and compare it with the conventional method in the scenario with four sensing stations linked through a star network. We show that our protocol can estimate not only the specific parameter but also arbitrary linear combinations of the sensed parameters. To evaluate the estimation precision, we adopt Fisher information which provides the lower bound of variance of the parameter. In addition, we evaluate the precision of estimation in the presence of distribution loss by calculating the distribution success probability. As a result, our protocol achieves lower variance than the direct transmission in a lossy environment.

The paper is organized as follows. In Section II, we

* yoshihiro_u@keio.jp

describe the method of distribution of GHZ states and introduce the Fisher information as a measure of distributed sensing accuracy. Section III contains the main results of our analysis which a demonstration that our protocol can measure arbitrary linear combination of sensed parameters more precisely than the conventional method. We summarize and discuss the results in a wider context in Section IV. Finally, the Appendix contains details of some technical derivations.

II. METHODS

In this section, we define a loss-tolerant protocol for the distribution of GHZ states. We also define the Fisher information which we use to estimate the precision limit for quantum network sensing.

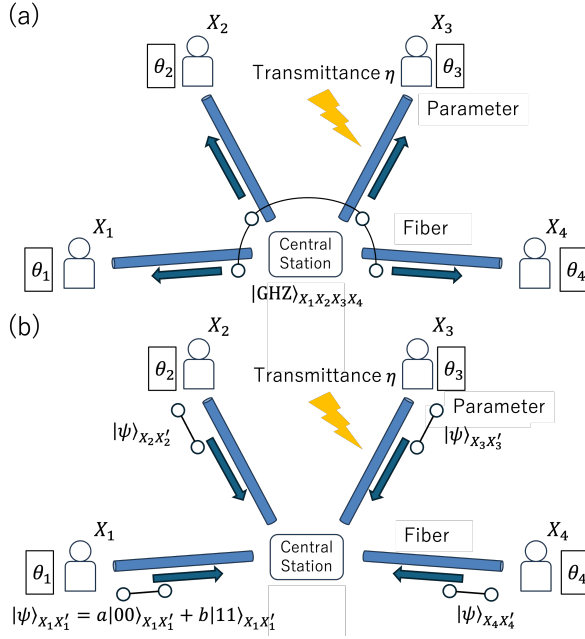


FIG. 1. A star network for estimation of functions of target parameters $\theta_1, \dots, \theta_4$ using distributed 4-partite entangled state $|\psi\rangle_{X_1X_2X_3X_4}$. The stations are denoted by X_1, \dots, X_4 . The sensing stations are connected with a central station with equal length optical links with transmittance η . (a) Direct transmission protocol. Generated GHZ state is transmitted to sensing stations via lossy channels. (b) Our scheme. Each station prepares a bi-partite photonic state $|\psi\rangle_{X_iX'_i}$ and sends one part to the central station, where the photons interfere and their states are measured in the photon number basis.

A. Efficient GHZ state distribution protocol

The GHZ state is a multi-partite entangled quantum state widely used in quantum protocols ranging from quantum cryptography to quantum sensing [19, 26, 33].

In the standard basis of two-level quantum systems (qubits) it is defined as a superposition of two perfectly aligned states of all systems. Let us give a definition for 4-qubits, which is relevant to our paper, and the extension of which is straightforward:

$$|\text{GHZ}\rangle = \frac{1}{\sqrt{2}}(|0000\rangle + |1111\rangle). \quad (1)$$

The phase between the terms is a matter of convention about how one defines the basis of particular systems, and does not reflect any essential properties of entanglement.

In quantum optical scenarios, including our work, the qubit is often defined in a two-dimensional subspace spanned by vectors of the photon number basis. In particular we consider the zero-photon state $|0\rangle$ and the one-photon state $|1\rangle$ as the optical qubit basis. In this convention, we can define a 4-partite GHZ state as follows [32]

$$|\text{GHZ}\rangle = \frac{1}{\sqrt{2}}(|1010\rangle - |0101\rangle). \quad (2)$$

The qubit and the optical photon-number qubit definitions are equivalent in the sense of formal definitions (up to renaming local basis elements), and in the operational sense, as in both cases an appropriate measurement can be constructed [34–38] which outcomes the same measurement statistics.

Let us introduce GHZ state distribution protocols. We consider a star network shown in Fig. 1. The parameters $\theta_1, \dots, \theta_4$ and sensing stations X_1, \dots, X_4 are separated from each other. In the direct transmission scenario, Fig. 1 (a), which is our reference, the GHZ state (2) is generated by the central node and distributed to each station via an optical fiber characterized by transmittance η . Let us notice that in this scenario the GHZ state is encoded in the polarization qubit basis, $|\leftrightarrow\rangle = |0\rangle$, $|\updownarrow\rangle = |1\rangle$,

$$|\text{GHZ}\rangle = \frac{1}{\sqrt{2}}(|\updownarrow\leftrightarrow\updownarrow\leftrightarrow\rangle - |\leftrightarrow\updownarrow\leftrightarrow\updownarrow\rangle). \quad (3)$$

It is necessary to distribute all photons to the appropriate stations. Therefore, the distribution success probability decreases exponentially as η^M , where M is the number of sensing stations.

To reduce the effect of loss in the distribution protocol, an efficient GHZ state distribution scheme was proposed by Shimizu et. al. [32]. The probability of success scales as $\eta^{\frac{M}{2}}$, which is a quadratic improvement with respect to the direct transmission. This method can be applied to an arbitrary even number of users M . Here, we consider $M = 4$ stations which sense $d = 4$ parameters.

In our scenario, each sensing station prepares a bi-partite state

$$|\psi\rangle_{X_iX'_i} = a|00\rangle + b|11\rangle \quad (4)$$

where $|a|^2 + |b|^2 = 1$. Here, X_i and X'_i denote the subsystems associated with the i -th node. The setup of the central node is shown in Fig. 2. State (4) can be generated

in a photonic or atomic system. In our case, the qubit in the photon-number basis $|0\rangle_{X'_i}$ and $|1\rangle_{X'_i}$ is transmitted to the central node. At the central node, the transmitted qubits interfere with each other and the output state is measured in the photon-number basis. Each observation in the measurement of subsystems $X'_1 X'_2 X'_3 X'_4$ results in collapsing the system $X_1 X_2 X_3 X_4$ to some state. The setup from Fig. 2 was used before to generate the W and Dicke states [39]. A few measurement results lead to formation of a GHZ state in the sensing stations [32].

To illustrate this mechanism, let us consider an example starting with the ideal lossless case and noiseless detectors. If two detectors signalize detection, we know that only two photons arrive at this stage; however, we do not know which systems generated those photons. Therefore, the resulting state, after the measurement, is a superposition of possible scenarios. For instance, if the 1st and 2nd detectors signalize photons, we succeed in generating GHZ state expressed by

$$|\text{GHZ}\rangle_4 = \frac{1}{\sqrt{2}} (|1010\rangle_{X_1 X_2 X_3 X_4} - |0101\rangle_{X_1 X_2 X_3 X_4}). \quad (5)$$

Depending on the detection pattern, we can also generate different states which, up to local basis renaming or a local phase flip are equivalent to the GHZ states. These states are listed in Table I.

In general, considering possibility of losses, after a successful detection event, the generated state can be described as a mixed state

$$\rho_{\text{CS}} = p |\text{GHZ}\rangle \langle \text{GHZ}|_4 + \sum_i r_i |\psi_i\rangle \langle \psi_i|, \quad (6)$$

where $|\psi_i\rangle$ are some undesirable states that are orthogonal to $|\text{GHZ}\rangle$. Here $p + \sum r_i = 1$.

In the quantum network sensing context, the distributed state that can be generated in this way can be additionally parametrized by independent unknown phase-shift parameters θ_i , where $i = 1, \dots, 4$. Our goal is to estimate some global parameter θ which is a function of the local parameters θ_i . In fact, our protocol can estimate different θ depending on generated GHZ states, which we distinguish based on the detector patterns. For instance, if the generated state is as in Eq. (5), we can estimate $\theta = \frac{1}{4}(\theta_1 - \theta_2 + \theta_3 - \theta_4)$, as we will explain later.

In this analysis, without loss of generality, we focus our attention on $\frac{1}{\sqrt{2}}(|1010\rangle - |0101\rangle)$ as the generated state and the target parameter $\theta = \frac{1}{4}(\theta_1 - \theta_2 + \theta_3 - \theta_4)$. In this case, the final state, after appropriate pattern of

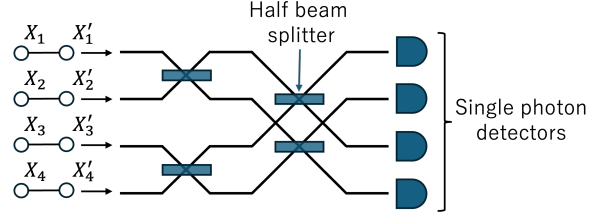


FIG. 2. Configuration of central node. Each station sends one of the photon pair to the central node and these transmitted photons are interfered with the interferometer constructed by the half beam splitter and are detected by the single photon detectors.

detectors signalizes photons, is as follows:

$$\begin{aligned} \rho_{\text{CS},\theta} &= p U_\theta |\text{GHZ}\rangle \langle \text{GHZ}| U_\theta^\dagger + \sum_i r_i |\psi_i\rangle \langle \psi_i| \\ &= \frac{1}{2} p (|1010\rangle \langle 1010| - e^{i4\theta} |1010\rangle \langle 0101| \\ &\quad - e^{-i4\theta} |0101\rangle \langle 1010| + |0101\rangle \langle 0101|) \\ &\quad + \sum_i r_i |\psi_i\rangle \langle \psi_i|, \end{aligned} \quad (7)$$

where U_θ is the unitary operator representing a phase shift, which acting in the photon-number basis $\{|0\rangle, |1\rangle\}$ is given as

$$\begin{aligned} U_\theta &= U_{\theta_1} \otimes U_{\theta_2} \otimes U_{\theta_3} \otimes U_{\theta_4} \\ &= \begin{bmatrix} 1 & 0 \\ 0 & e^{i\theta_1} \end{bmatrix} \otimes \begin{bmatrix} 1 & 0 \\ 0 & e^{i\theta_2} \end{bmatrix} \otimes \begin{bmatrix} 1 & 0 \\ 0 & e^{i\theta_3} \end{bmatrix} \otimes \begin{bmatrix} 1 & 0 \\ 0 & e^{i\theta_4} \end{bmatrix}. \end{aligned} \quad (8)$$

The undesirable states $|\psi_i\rangle \langle \psi_i|$ in (7) are diagonal, so they do not carry any information about θ . We can estimate the lower bound of the variance of parameter $\Delta\theta^2$ by calculating the Fisher information. We explain it in the next section, where we introduce the notion of the Quantum and classical Fisher information.

TABLE I. States $|\Phi\rangle_{X_1, \dots, X_4}$ in subsystems $X_1 \dots X_4$ depending on detection pattern in subsystems $X'_1 \dots X'_4$ [32].

Detection pattern	State $ \Phi\rangle_{X_1, \dots, X_4}$
1,2	$\frac{1}{\sqrt{2}}(1010\rangle - 0101\rangle)$
1,3	$\frac{1}{\sqrt{2}}(1100\rangle - 0011\rangle)$
1,4	$\frac{1}{\sqrt{2}}(1001\rangle - 0110\rangle)$
2,3	$\frac{1}{\sqrt{2}}(- 1001\rangle + 0110\rangle)$
2,4	$\frac{1}{\sqrt{2}}(- 1100\rangle + 0011\rangle)$
3,4	$\frac{1}{\sqrt{2}}(- 1010\rangle + 0101\rangle)$

B. Parameter estimation limit: classical and quantum Fisher information

Precision in parameter estimation is quantified by the estimator variance $\Delta\theta^2$, which is derived from measured

parameters θ_{est} and associated probability function $P = \{P_1, P_2, \dots, P_i\}$. The variance $\Delta\theta^2$ is defined as follows:

$$\Delta\theta^2 = \langle (\theta_{\text{est}} - \theta)^2 \rangle. \quad (9)$$

From the probability function P , we can construct the lower bound called the classical Cramér-Rao Bound,

$$\Delta\theta^2 \geq \frac{1}{NF_{C\theta}[P]}, \quad (10)$$

where $F_{C\theta}$ is the classical Fisher information (CFI) of θ and N is the number of repetitions [4]. CFI of θ is derived from the classical Fisher information Matrix (CFIM) \mathbf{F}_C , defined as follows:

$$(\mathbf{F}_C[P])_{kl} = \sum_i \frac{1}{P_i} \left(\frac{\partial P_i}{\partial \theta_k} \right) \left(\frac{\partial P_i}{\partial \theta_l} \right). \quad (11)$$

For combinations of parameters,

$$F_{C\theta}[P] = \frac{\mathbf{w}^T \mathbf{F}_C \mathbf{w}}{(\mathbf{w}^T \mathbf{w})^2} \quad (12)$$

where \mathbf{w} is the vector of weighted coefficients w_i in the combination. To calculate the CFI for a parameter θ encoded in a shared entangled state (7) and measured by local sensing stations, we need to define a measurement operators applied by each sensing station independently. It is known [26] that in such we consider, the measurement defined by the projectors on the eigenvectors of the Pauli operator σ_x

$$\begin{aligned} \sigma_{x+} &= \frac{1}{\sqrt{2}}(|0\rangle + |1\rangle), \\ \sigma_{x-} &= \frac{1}{\sqrt{2}}(|0\rangle - |1\rangle), \end{aligned} \quad (13)$$

is optimal to achieve the minimum of $\frac{1}{F_C[P]}$.

However, this measurement is particularly problematic in the photon-number qubit basis, as it requires intermediate interaction between the photon and matter, for example, in quantum memory, or other sophisticated techniques which may make our procedure less feasible with the current technology. Therefore, instead of σ_x basis measurement, we consider the measurement defined by displacement followed by photon counting [34, 35]. This situation is schematically shown in Fig. 3. Thus, our local measurement operators $M_{i,0}$ and $M_{i,1}$ which we propose to extract information about the global parameter θ from the shared entangled state (7) are:

$$M_{i,0} = |\alpha\rangle \langle \alpha|, M_{i,1} = I - |\alpha\rangle \langle \alpha|, \quad (14)$$

where I is the identity matrix and $|\alpha\rangle$ the coherent state $|\alpha\rangle = e^{-\frac{1}{2}|\alpha|^2} \sum_{n=0}^{\infty} \frac{\alpha^n}{\sqrt{n!}} |n\rangle$. We assume that the coherent state can be approximated by its expansion in the photon-number qubit basis $|\alpha\rangle \approx e^{-\frac{1}{2}|\alpha|^2} (|0\rangle + \alpha|1\rangle)$.

Based on such a measurement, we can construct the probability function P for joint detection events of all stations from the four-fold coincidence events. We number these events by $k \in \{0, 2^4 - 1\}$, where each event signalizes a pattern composed of local measurements M_{i,k_i} and k_i is 0 or 1. Thus, P_k can be expressed as

$$P_k = \text{Tr}[\rho_\theta M_{1,k_1} \otimes M_{2,k_2} \otimes M_{3,k_3} \otimes M_{4,k_4}]. \quad (15)$$

The index $k \in \{0, 2^4 - 1\}$ in its binary representation is $(k_1 k_3 k_3 k_4)$ and $\rho_\theta = U_\theta |\text{GHZ}\rangle \langle \text{GHZ}|_4 U_\theta^\dagger$.

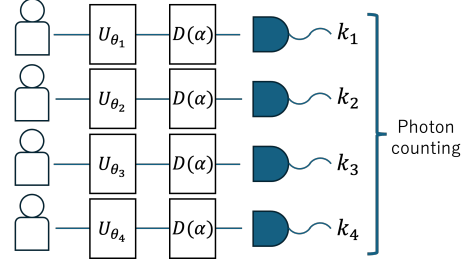


FIG. 3. Measurement setup for extracting information about a global parameter θ from coincidences in the local measurements given by displacement and photon counting. The measured state is the shared global state.

As mentioned before, CFI specifies the lower bound on the variance of the estimated parameter. However, how close one can approach this bound depends on how the parameter is measured. The optimal measurement for photon-number qubit in terms of current feasible technology is unknown. The quantum Fisher information (QFI) and quantum Cramér-Rao Bound (QCRB) give another theoretically achievable in quantum mechanics lower bound on the variance of parameters encoded in quantum states with non-local quantum correlations. Similar to (10), QCRB is given by

$$\Delta\theta^2 \geq \frac{1}{NF_{Q\theta}[\rho_\theta]}, \quad (16)$$

where $F_{Q\theta}$ is the QFI of θ and ρ_θ is the density matrix parametrized by θ . If ρ_θ is a pure state $\rho_\theta = |\psi_\theta\rangle \langle \psi_\theta|$, $F_{Q\theta}$ can be computed based on the quantum Fisher information Matrix (QFIM) \mathbf{F}_Q as follows [4, 40]:

$$(\mathbf{F}_Q[\rho_\theta])_{kl} = 4\text{Re}(\langle \partial_{\theta_k} \psi_\theta | \partial_{\theta_l} \psi_\theta \rangle - \langle \partial_{\theta_k} \psi_\theta | \psi_\theta \rangle \langle \psi_\theta | \partial_{\theta_l} \psi_\theta \rangle) \quad (17)$$

as follows

$$F_{Q\theta}[\rho_\theta] = \frac{\mathbf{w}^T \mathbf{F}_Q \mathbf{w}}{(\mathbf{w}^T \mathbf{w})^2}, \quad (18)$$

where $|\partial_{\theta_k} \psi_\theta\rangle = \frac{\partial}{\partial \theta_k} |\psi_\theta\rangle$. By using the above equations, we derive QFI and CFI.

For the direct transmission protocol, we only use the pure GHZ state, because (ignoring the detectors dark counts) it can be verified by all photons being detected. So, the parametrized GHZ state becomes simply:

$$\rho_{D,\theta} = U_\theta |\text{GHZ}\rangle \langle \text{GHZ}| U_\theta^\dagger, \quad (19)$$

where GHZ state is (2) but in the polarization qubit basis. To calculate CFI, we choose the σ_x basis measurement (13). Following (18), the QFI of this state reads

$$(\mathbf{F}_Q[\rho_{D,\theta}])_{kl} = 1, \quad (20)$$

if $k = l$ or both k and l are even or odd; or

$$(\mathbf{F}_Q[\rho_{D,\theta}])_{kl} = -1, \quad (21)$$

if k is even and l is odd or k is odd and l is even. Hence

$$F_{Q\theta}[\rho_{D,\theta}] = 16. \quad (22)$$

When we project state (19) onto the σ_x basis, we can get two patterns of the probability of four coincident detection events depending on θ which are expressed as

$$P_1 = \frac{1}{16} (1 + \cos 4\theta), \quad P_2 = \frac{1}{16} (1 - \cos 4\theta), \quad (23)$$

where 1 corresponds to measurement pattern (0101) and 2 to (1010).

From (12), CFIM and CFI of (19) are expressed as

$$\begin{aligned} (\mathbf{F}_C[\rho_{D,\theta}])_{kl} &= 8 \times \frac{16}{1 + \cos 4\theta} \left(\frac{\sin 4\theta}{16} \right)^2 \\ &+ 8 \times \frac{16}{1 - \cos 4\theta} \left(\frac{\sin 4\theta}{16} \right)^2 \\ &= 8 \left[\frac{\sin^2 4\theta (1 - \cos 4\theta) + \sin^2 4\theta (1 + \cos 4\theta)}{16 \times (1 - \cos^2 4\theta)} \right] \\ &= 8 \times \frac{1 - \cos 4\theta + 1 + \cos 4\theta}{16} = 1, \end{aligned} \quad (24)$$

if $k = l$ or both k and l are even or odd; and

$$\begin{aligned} (\mathbf{F}_C[\rho_{D,\theta}])_{kl} &= 8 \times \frac{16}{1 + \cos 4\theta} \left(\frac{\mp \sin 4\theta}{16} \right) \left(\frac{\pm \sin 4\theta}{16} \right) \\ &+ 8 \times \frac{16}{1 - \cos 4\theta} \left(\frac{\pm \sin 4\theta}{16} \right) \left(\frac{\mp \sin 4\theta}{16} \right) \\ &= 8 \left[\frac{-\sin^2 4\theta (1 - \cos 4\theta) - \sin^2 4\theta (1 + \cos 4\theta)}{16 \times (1 - \cos^2 4\theta)} \right] \\ &= 8 \times \frac{-1 + \cos 4\theta - 1 - \cos 4\theta}{16} = -1, \end{aligned} \quad (25)$$

if k even and l is odd or k odd and l is even. Hence

$$F_{C\theta} = \frac{\mathbf{w}^T \mathbf{F}_C[\rho_{D,\theta}] \mathbf{w}}{(\mathbf{w}^T \mathbf{w})^2} = 16, \quad (26)$$

where $\mathbf{w} = \{\frac{1}{4}, -\frac{1}{4}, \frac{1}{4}, -\frac{1}{4}\}$. Therefore, we showed that $F_Q[\rho_{D,\theta}] = F_C[\rho_{D,\theta}]$.

In our scheme, the parametrized state is expressed by (7). Because QFI is a convex function, we transform (18)

with state (7) as follows:

$$\begin{aligned} \mathbf{F}_Q[\rho_{CS,\theta}] &= \mathbf{F}_Q \left[p U_\theta |\text{GHZ}\rangle \langle \text{GHZ}| U_\theta^\dagger + \sum_i r_i |\psi_i\rangle \langle \psi_i| \right] \\ &\leq p \mathbf{F}_Q \left[U_\theta |\text{GHZ}\rangle \langle \text{GHZ}| U_\theta^\dagger \right] + \sum_i r_i \mathbf{F}_Q[|\psi_i\rangle \langle \psi_i|]. \end{aligned} \quad (27)$$

Definition (18) implies that the quantum Fisher information of the term which does not include the component of θ is zero. Thus, we get the information about θ from the first term of (27) only:

$$\mathbf{F}_Q[\rho_{CS,\theta}] \leq p \mathbf{F}_Q[U_\theta |\text{GHZ}\rangle \langle \text{GHZ}|_4 U_\theta^\dagger], \quad (28)$$

which implies

$$F_{Q\theta}[\rho_{CS,\theta}] \leq p \times \frac{\mathbf{w}^T \mathbf{F}_Q[\rho_{CS,\theta}] \mathbf{w}}{(\mathbf{w}^T \mathbf{w})^2} = 16p. \quad (29)$$

To calculate the classical Fisher information of our scheme considering the measurement (14), we get the probabilities of several possible coincidence detection events. In contrast to the direct transmission, we can get nontrivial patterns. The results are discussed in Section III.

C. Arbitrary linear combination of the parameters

In this section, we show that our protocol allows us to estimate the parameter $\hat{\theta}$ which is described by an arbitrary linear combination of the parameters $\hat{\theta} = \sum_i^d w_i \theta_i$ when one of the modes is a reference. As an example, we consider the situation where $N = 4$, $d = 3$ and the fourth mode is the reference.

As shown in Table I, different GHZ states are generated depending on the detection patterns which implies that we can estimate different functions which are shown in Table II. By combining the estimated parameters, we can estimate an arbitrary linear combination of the parameters. In particular, phases $\theta_1 \sim \theta_3$ can be expressed as functions of $\theta_{P1+}, \theta_{P2+}, \theta_{P3-}$ which are estimated directly from the experiment:

$$\theta_1 = \frac{\theta_{P1+} + \theta_{P2+}}{2}, \theta_2 = \frac{\theta_{P2+} + \theta_{P3-}}{2}, \theta_3 = \frac{\theta_{P1+} + \theta_{P3-}}{2}. \quad (30)$$

Thus, we can estimate the linear combinations parameter $\hat{\theta}$ by collecting the estimators of parameters of GHZ states obtained when Patterns 1~3 are observed. Components θ_{P1+} , θ_{P2+} and θ_{P3-} are estimated independently, so the variance $\Delta \hat{\theta}^2$ is the sum of the variances of the parameters, as shown in Appendix B.

III. RESULTS

We calculate QCRB and CCRB for the scenario with $M = 4$ sensing stations and $d = 4$ parameters. We as-

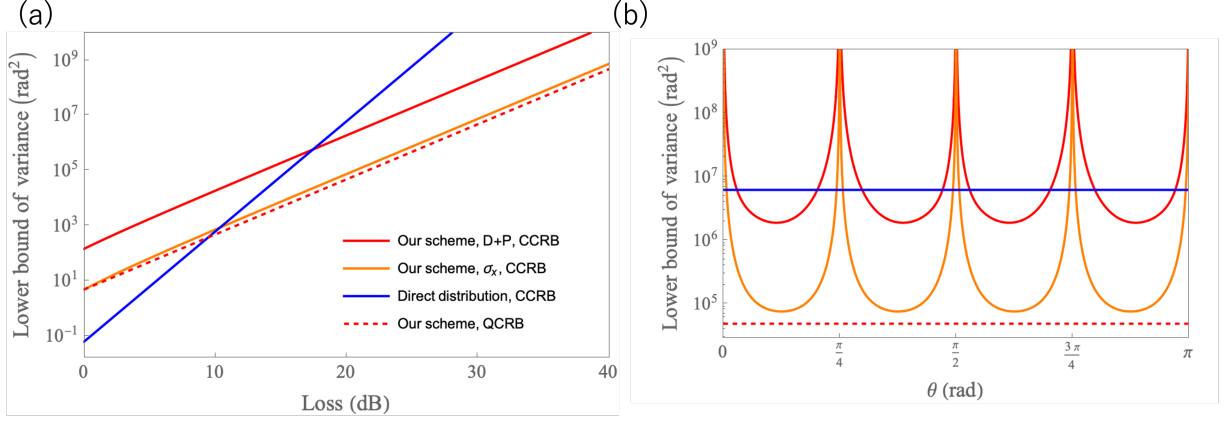


FIG. 4. Lower bound of variance derived by QCRB and CCRB. QCRB of our protocol is shown as red dotted line. Our protocol measured by displacement and photon counting is shown as red line. Our protocol in which the qubits are projected onto the σ_x basis is shown as orange line. Blue line shows the CCRB of Direct distribution. (a) The lower bound of variance versus distribution loss when $\theta = \frac{\pi}{8}$. (b) The lower bound of variance versus the sensed phase $\theta = \frac{1}{4}(\theta_1 - \theta_2 + \theta_3 - \theta_4)$ when the distribution loss is 20 dB.

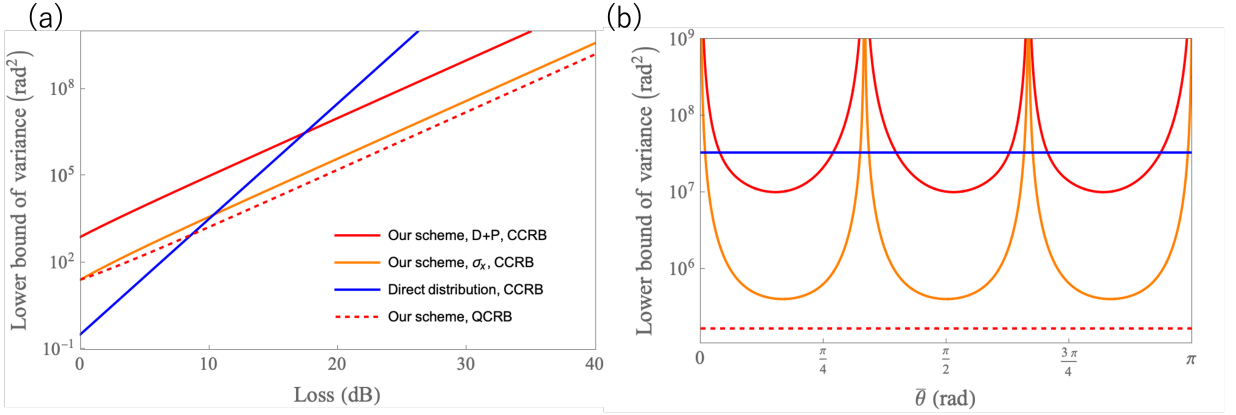


FIG. 5. The result when the sensed parameter is the average of phases $\bar{\theta} = \frac{1}{3}(\theta_1 + \theta_2 + \theta_3)$. We assume that we get each detection patterns shown in Table.II 30 times. (a) The lower bound of variance versus distribution loss when $\bar{\theta} = \frac{\pi}{6}$. (b) The lower bound of variance versus the sensed phase $\bar{\theta} = \frac{1}{4}(\theta_1 + \theta_2 + 2\theta_3)$ when the distribution loss is 20 dB.

TABLE II. The phases which our protocol can estimate.

Detection pattern	The phases
Pattern 1: {1,2} or {3,4}	$\{\theta_{P1+} = \theta_1 - \theta_2 + \theta_3\}$ or
	$\{\theta_{P1-} = -\theta_1 + \theta_2 - \theta_3\}$
Pattern 2: {1,3} or {2,4}	$\{\theta_{P2+} = \theta_1 + \theta_2 - \theta_3\}$ or
	$\{\theta_{P2-} = -\theta_1 - \theta_2 + \theta_3\}$
Pattern 3: {1,4} or {2,3}	$\{\theta_{P3+} = \theta_1 - \theta_2 - \theta_3\}$ or
	$\{\theta_{P3-} = -\theta_1 + \theta_2 + \theta_3\}$

sume that transmittance $\eta = 0.2$ [db/km], where L is the distance from a central node, repetition N is 1, and we set the displacement parameter α as $\frac{1}{\sqrt{2}}$ which corresponds to the minimum CCRB. Fig. 4, shows the

results for the parameter $\theta = \frac{1}{4}(\theta_1 - \theta_2 + \theta_3 - \theta_4)$, which is estimated if the detection signalizes generation of $|\psi\rangle = \frac{1}{\sqrt{2}}(|1010\rangle - |0101\rangle)$. We compare the performance of our scheme with the conventional method—direct transmission. The probability function P is constructed based on four-coincidence events of the σ_x measurements in the local stations.

For precision evaluation including the distribution loss, we assume the number of the valid measurement N' as follows:

$$N' = N \times P_{suc} \quad (31)$$

where P_{suc} is the success probability of GHZ state distribution. The details are shown in Appendix A 1.

As we mentioned in Section II A, the QCRB and CCRB in our scheme are calculated using displacement and photon counting. For comparison, in our presenta-

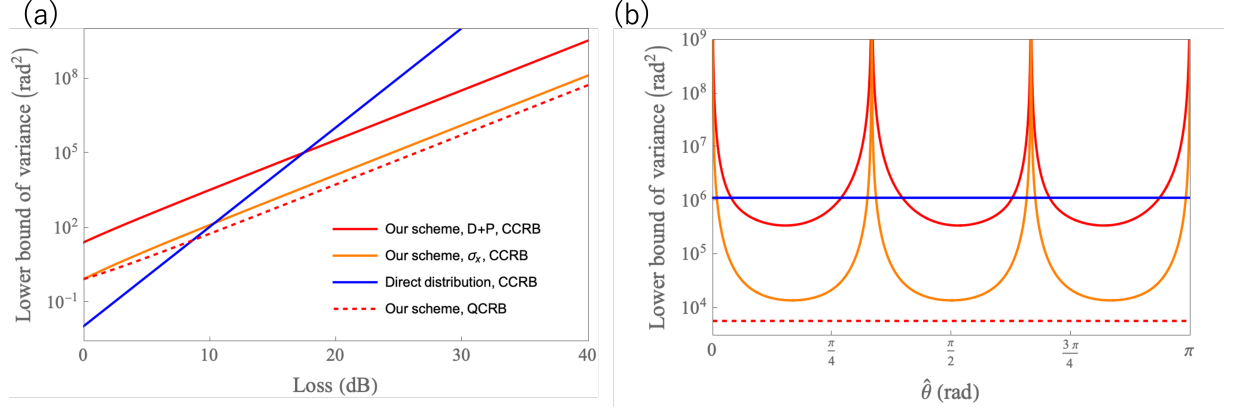


FIG. 6. The result when the sensed parameter is arbitrary linear combination of phases. This figure is plotted when the sensed phase $\hat{\theta}$ is $\hat{\theta} = \frac{1}{4}(\theta_1 + \theta_2 + 2\theta_3)$. As same as Fig.[5], we assume that we get each detection patterns shown in Table.II 30 times.(a) The lower bound of variance versus distribution loss when $\hat{\theta} = \frac{\pi}{6}$. (b) The lower bound of variance versus the sensed phase $\hat{\theta}$ when the distribution loss is 20 dB.

tion, we also calculate the quantities considering σ_x basis measurement as the ideal case.

Moreover, we derive the QCRB and CCRB when one of the modes is a reference. The results are shown in Fig. 5 and Fig. 6. The parameter is $\bar{\theta} = \frac{1}{3}(\theta_1 + \theta_2 + \theta_3)$ in Fig. 5, and $\hat{\theta} = \frac{1}{4}(\theta_1 + \theta_2 + 2\theta_3)$ in Fig. 6. We assume that three GHZ states, which are shown in Table I, are generated N times, where $N = 30$. These parameters are chosen to demonstrate some typical situations. Similar to Fig. 4, we compare our scheme with the direct transmission scheme with the corresponding states. To calculate the QCRB and CCRB of direct distribution, we assume that the same three GHZ states as our scheme are sent $N = 30$ times.

Fig. 4, 5, 6 (a) show that our scheme has an advantage in the scaling of the variance. On the other hand, CCRB of our scheme does not reach QCRB. In the ideal case of our scheme, using σ_x basis measurement, CCRB reaches the QCRB when there is no loss but it does not reach it in a presence of loss. It means that σ_x basis measurement is not optimal for noisy states.

Fig. 4, 5, 6 (b) show that the variance depends on the estimation parameters. Our scheme provides more precise estimation than the alternative method. However, as in Fig. 4, 5, 6 (a), CCRB does not reach QCRB. Additionally, for specific phases the variance diverges. The range at which the variance diverges increases when the number of phases increases, so that this phenomenon seems critical for the distributed sensing scenario.

The parameters a and b in (4) we have chosen as follows: $a = \sqrt{0.8}$ and $b = \sqrt{0.2}$ which give a reasonable fidelity and rate of the generated GHZ state [32].

IV. CONCLUSIONS AND OUTLOOK

We propose the quantum network sensing protocol using robust multi-partite entanglement distribution and calculate the Quantum and classical CRB. We show that our protocol achieves lower variance of estimation than the reference conventional method in the regime of high loss. On the other hand, compared with conventional method, CCRB in our scheme does not achieve QCRB.

To approach QCRB, we may consider possible extensions of the scheme including optimization of the measurement and alternative choices of the probe states. Regarding the measurement optimization, The σ_x basis measurement is known as the measurement which can achieve QCRB in the ideal situation, but when the noisy state appears, it remains suboptimal. Furthermore, we cannot estimate certain phases because the variance becomes infinite, as shown in Fig. 4, 5, 6 (b). Moreover, for CCRB to better approach QCRB we need to construct the measurement scheme which is robust against noise.

Other than GHZ entangled states can be also useful in the quantum network sensing context. Recent research [41] suggests that symmetric Dicke states are robust against noise and enable more precise estimation than GHZ state. The protocol we consider here is flexible and can be adapted to generate not only GHZ state, but also Dicke states depending on the measurement pattern [39]. For quantum network sensing applications, it is necessary to investigate the optimal quantum setups further.

In this work, we assume that the reference conventional method—direct transmission—can generate pure GHZ state deterministically, so that CCRB achieves the QCRB. However, in realistic situations, this method sometimes generate noisy GHZ states or fails to generate. In this work we idealize the reference method to search for the worst case advantages of our scheme. Indeed, we

calculate QCRB and CCRB including the noise in the generation step and the success probability of GHZ state generation in our method. As expected and shown in our results and [41], the variance increases if the used states are noisy. For more realistic comparison it is reasonable to calculate CCRB including the noise and generation rate also in the reference method.

Also, as a proof of principle, we consider a 4-parameter problem. Nevertheless, our scheme can be extended beyond that number. The direction of further studies would be to look for the Heisenberg scaling against the number of sensing stations M . Increasing this number could be essential in future applications. It is known that, due to fiber loss, the success probability of entangled state sharing is exponentially decreasing when M increases. However, as shown in the Results section, our scheme is relatively robust against fiber loss as the scaling of the success rate is $\eta^{\frac{M}{2}}$. These features support our confidence that the scheme proposed here is effective for future applications.

ACKNOWLEDGMENTS

This work was supported by JST Moonshot *R&D*, Grant No. JPMJMS226C and Grant No. JPMJMS2061, JST CRONOS, Grant No. JPMJCS24N6, JST SPRING, Grant No. JPMJSP2123, JST ASPIRE, Grant No. JPMJAP2427, JST COI-NEXT Grant No. JPMJPF2221 and Program for the Advancement of Next Generation Research Projects, Keio University.

Appendix A: Appendixes

1. Success probability of GHZ state generation

Here we show the calculation of the success probability of four-partite GHZ state generation. As we mentioned before, distribution process in the direct transmission method, which is our reference, records a success if all photons arrive at the end stations. Therefore, the success probability is η^4 .

In our scheme, GHZ state is generated when we get the target detection pattern from single photon detectors.

According to [32], this probability is

$$\begin{aligned} P_{CS} &= 2 \sum_{m=0}^{\frac{N}{2}} \eta^{\frac{N}{2}} (1-\eta)^m \left(\frac{1}{2}\right)^{\frac{3}{2}N-5} \\ &\times a^{N-2m} b^{N+2m} \frac{N}{2} C_m \\ &= \left(\frac{1}{2}\right)^{\frac{3}{2}N-5} \eta^{\frac{N}{2}} b^N [a^2 + b^2(1-\eta)]^{\frac{N}{2}}. \end{aligned} \quad (A1)$$

where m is the number of photons which is lost in the fiber. Equation (A1) takes into account the situation when photon loss can occur. Specifically, we get the target detection pattern, with probabilities

$$\begin{aligned} P_{CS,0} &= \eta^{\frac{N}{2}} \left(\frac{1}{2}\right)^{\frac{3}{2}N-4} a^N b^N, \\ P_{CS,1} &= \eta^{\frac{N}{2}} (1-\eta)^1 \left(\frac{1}{2}\right)^{\frac{3}{2}N-4} a^{N-2} b^{N+2}, \\ P_{CS,2} &= \eta^{\frac{N}{2}} (1-\eta)^2 \left(\frac{1}{2}\right)^{\frac{3}{2}N-4} a^{N-4} b^{N+2}, \end{aligned} \quad (A2)$$

with the number of photons lost indicated by the the subscript. From (A1) and (A2), the rates-parameters of the noisy GHZ state taken into account in the paper α_{GHZ}, β_i are given by

$$p = \frac{P_{CS,0}}{P_{CS}}, \quad r_1 = \frac{P_{CS,1}}{P_{CS}}, \quad r_2 = \frac{P_{CS,2}}{P_{CS}}. \quad (A3)$$

2. Analysis of the variance of $\hat{\theta}$

As we mentioned in the main text, our scheme allows us to estimate an arbitrary linear combination of the parameters θ and $\hat{\theta}$. In this section, we show how to calculate the variance of $\hat{\theta}$ and $\hat{\theta}$. According to Eq. (30) and standard statistical analysis, the variance $\Delta \hat{\theta}^2$ is expressed as follows:

$$\begin{aligned} \Delta \hat{\theta}^2 &= V[\hat{\theta}] \\ &= V \left[w_1 \left(\frac{\theta_{P1+} + \theta_{P2+}}{2} \right) + w_2 \left(\frac{\theta_{P2+} + \theta_{P3-}}{2} \right) \right. \\ &\quad \left. + w_1 \left(\frac{\theta_{P1+} + \theta_{P3-}}{2} \right) \right] \\ &= \left(\frac{w_1 + w_2}{2} \right)^2 \Delta \theta_{P1+}^2 + \left(\frac{w_2 + w_3}{2} \right)^2 \Delta \theta_{P2+}^2 \\ &\quad + \left(\frac{w_1 + w_3}{2} \right)^2 \Delta \theta_{P3-}^2 \end{aligned} \quad (A4)$$

where $V[\hat{\theta}]$ is the variance of $\hat{\theta}$.

-
- [1] C. L. Degen, F. Reinhard, and P. Cappellaro, Quantum sensing, *Rev. Mod. Phys.* **89**, 035002 (2017).
 - [2] V. Giovannetti, S. Lloyd, and L. Maccone, Quantum-enhanced measurements: Beating the standard quantum limit, *Science* **306**, 1330 (2004).
 - [3] S. Pirandola, B. Bardhan, T. Gehring, *et al.*, Advances in photonic quantum sensing, *Nat. Photonics* **12**, 724–733 (2018).
 - [4] R. Demkowicz-Dobrzański, M. Jarzyna, and J. Kołodyński, Chapter four - quantum limits in optical interferometry, in *Progress in Optics*, Vol. 60, edited by E. Wolf (Elsevier, 2015) pp. 345–435.
 - [5] K. Qian, Z. Eldredge, W. Ge, *et al.*, Heisenberg-scaling measurement protocol for analytic functions with quantum sensor networks, *Phys. Rev. A* **100**, 042304 (2019).
 - [6] T. Ono, R. Okamoto, and S. Takeuchi, An entanglement-enhanced microscope, *Nat. Commun.* **4**, 2426 (2013).
 - [7] T. L. S. Collaboration, Enhanced sensitivity of the ligo gravitational wave detector by using squeezed states of light, *Nat. Photonics* **7**, 613–619 (2013).
 - [8] Z. Zhang and Q. Zhuang, Distributed quantum sensing, *Quantum Sci. Technol.* **6**, 043001 (2021).
 - [9] T. J. Proctor, P. A. Knott, and J. A. Dunningham, Multiparameter estimation in networked quantum sensors, *Phys. Rev. Lett.* **120**, 080501 (2018).
 - [10] Y. Yang, B. Yadin, and Z.-P. Xu, Quantum-enhanced metrology with network states, *Phys. Rev. Lett.* **132**, 210801 (2024).
 - [11] V. Giovannetti, S. Lloyd, and Maccone, Quantum-enhanced positioning and clock synchronization, *Nature* **412**, 417–419 (2001).
 - [12] P. Kómár, E. Kessler, and M. a. o. Bishof, A quantum network of clocks, *Nat. Phys.* **10**, 582–587 (2014).
 - [13] D. Gottesman, T. Jennewein, and S. Croke, Longer-baseline telescopes using quantum repeaters, *Phys. Rev. Lett.* **109**, 070503 (2012).
 - [14] B. Purvis, R. Lafler, and R. N. Lanning, Practical approach to extending baselines of telescopes using continuous-variable quantum information, *New J. Phys.* **26**, 103006 (2024).
 - [15] E. T. Khabiboulline, J. Borregaard, K. De Greve, and M. D. Lukin, Optical interferometry with quantum networks, *Phys. Rev. Lett.* **123**, 070504 (2019).
 - [16] Q. Zhuang, Z. Zhang, and J. H. Shapiro, Distributed quantum sensing using continuous-variable multipartite entanglement, *Phys. Rev. A* **97**, 032329 (2018).
 - [17] Q. Zhuang, J. Preskill, and L. Jiang, Distributed quantum sensing enhanced by continuous-variable error correction, *New J. Phys.* **22**, 022001 (2020).
 - [18] L. Pezzè and A. Smerzi, Distributed quantum multiparameter estimation with optimal local measurements (2024), arXiv:2405.18404 [quant-ph].
 - [19] D. Kim, S. Hong, Y. Kim, *et al.*, Distributed quantum sensing of multiple phases with fewer photons, *Nat. Commun.* **15**, 266 (2024).
 - [20] P. C. Humphreys, M. Barbieri, A. Datta, and I. A. Walmsley, Quantum enhanced multiple phase estimation, *Phys. Rev. Lett.* **111**, 070403 (2013).
 - [21] J. J. Bollinger, W. M. Itano, D. J. Wineland, and D. J. Heinzen, Optimal frequency measurements with maximally correlated states, *Phys. Rev. A* **54**, R4649 (1996).
 - [22] D. Greenberger, M. Horne, A. Shimony, and A. Zeilinger, Bell’s theorem without inequalities, *Am. J. Phys.* **58**, 1131 (1990).
 - [23] X. Guo, C. Breum, J. Borregaard, *et al.*, Distributed quantum sensing in a continuous-variable entangled network, *Nat. Phys.* **16**, Nat. Phys. (2020).
 - [24] Y. Xia, W. Li, W. Clark, *et al.*, Demonstration of a reconfigurable entangled radio-frequency photonic sensor network, *Phys. Rev. Lett.* **124**, 150502 (2020).
 - [25] S. Hong, J. ur Rehman, Y. Kim, *et al.*, Quantum enhanced multiple-phase estimation with multi-mode n00n states, *Nat. Commun.* **12**, 5211 (2021).
 - [26] L. Liu, Y. Zhang, Z. Li, *et al.*, Distributed quantum phase estimation with entangled photons, *Nat. Photonics* **15**, 137–142 (2021).
 - [27] J. Zhang, L. Wang, Y.-J. Hai, *et al.*, Distributed multiparameter quantum metrology with a superconducting quantum network (2024), arXiv:2412.18398 [quant-ph].
 - [28] S. Daryanoosh, S. Slussarenko, D. Berry, *et al.*, Experimental optical phase measurement approaching the exact heisenberg limit, *Nat. Commun.* **4606**, 4606 (2018).
 - [29] Y. M. Zhang, X. W. Li, W. Yang, and G. R. Jin, Quantum fisher information of entangled coherent states in the presence of photon loss, *Phys. Rev. A* **88**, 043832 (2013).
 - [30] A. Zang, A. Kolar, A. Gonzales, *et al.*, Quantum advantage in distributed sensing with noisy quantum networks (2024), arXiv:2409.17089 [quant-ph].
 - [31] P. Sekatski, S. Wölk, and W. Dür, Optimal distributed sensing in noisy environments, *Phys. Rev. Res.* **2**, 023052 (2020).
 - [32] H. Shimizu, W. Roga, D. Elkouss, and M. Takeoka, Simple loss-tolerant protocol for ghz-state distribution in a quantum network (2024), arXiv:2404.19458 [quant-ph].
 - [33] M. Proietti, J. Ho, F. Grasselli, P. Barrow, M. Malik, and A. Fedrizzi, Experimental quantum conference key agreement, *Sci. Adv.* **7**, eabe0395 (2021).
 - [34] M. Takeoka, M. Sasaki, P. van Loock, and N. Lütkenhaus, Implementation of projective measurements with linear optics and continuous photon counting, *Phys. Rev. A* **71**, 022318 (2005).
 - [35] M. Takeoka, M. Sasaki, and N. Lütkenhaus, Binary projective measurement via linear optics and photon counting, *Phys. Rev. Lett.* **97**, 040502 (2006).
 - [36] S. Asshab, K. Maruyama, and F. Nori, Detecting mode entanglement: The role of coherent states, superselection rules and particle statistics, *Phys. Rev. A* **76**, 052113 (2007).
 - [37] Y. Ota, S. Ashhab, and F. Nori, Implementing general measurements on linear optical and solid-state qubits, *Phys. Rev. A* **85**, 043808 (2012).
 - [38] D. P. Nadlinger, P. Drmota, B. C. Nichol, G. Araneda, D. Main, R. Srinivas, D. M. Lucas, C. J. Ballance, K. Ivanov, E. Y.-Z. Tan, P. Sekatski, R. L. Urbanke, R. Renner, N. Sangouard, and J.-D. Bancal, Experimental quantum key distribution certified by Bell’s theorem, *Nature* **607**, 682 (2022).
 - [39] W. Roga, R. Ikuta, T. Horikiri, and M. Takeoka, Efficient dicke-state distribution in a network of lossy channels, *Phys. Rev. A* **108**, 012612 (2023).
 - [40] J. Liu, H. Yuan, X.-M. Lu, and X. Wang, Quantum fisher information matrix and multiparameter estimation, *J.*

- Phys. A: Math. Theor. **53**, 023001 (2020).
- [41] Y. Cao and X. Wu, Distributed quantum sensing network with geographically constrained measurement strategies, in *ICASSP 2023 - 2023 IEEE International Conference on Acoustics, Speech and Signal Processing (ICASSP)* (2023) pp. 1–5.